Dragana Đurić · Ana Mladenović · Milica Pešić-Georgiadis · Miloš Marjanović · Biljana Abolmasov

Using multiresolution and multitemporal satellite data for post-disaster landslide inventory in the Republic of Serbia

Abstract This paper focuses on a specific event-based landslide inventory compiled after the May 2014 heavy rainfall episode in Serbia as a part of the post-disaster recovery actions. The inventory was completed for a total of 23 affected municipalities, and the municipality of Krupanj was selected as the location for a more detailed study. Three sources of data collection and analysis were used: a visual analysis of the post-event very high and high (VHR-HR) resolution images (Pléiades, WorldView-2 and SPOT 6), semi-automatic landslide recognition in pre- and post-event coarse resolution images (Landsat 8) and a landslide mapping field campaign. The results suggest that the visual and semi-automated analyses significantly contributed to the quality of the final inventory, including the associated planning strategies for conducting future field campaigns (as a final stage of the inventorying process), all the more so because the field-based and image-based inventories were focused on different types of landslides. In the most affected municipalities that had very high resolution satellite image coverage (19.52% of the whole study area), the density of the recognized landslides was approximately three times higher than that in those municipalities without satellite image coverage (where only field data were available). The total number of field-mapped landslides for the 23 municipalities was 1785, while image-based inventories, which were available only for the municipalities with satellite image coverage (77.43% of the study area), showed 1298 landslide records. The semi-automated landslide inventory in the test area (Krupanj municipality), which was based on coarse resolution multitemporal images (Landsat 8), counted 490 landslide instances and was in agreement with the visual analysis of the higher resolution images, with an overlap of approximately 40%. These results justify the use of preliminary inventorying via satellite image analysis and suggest a considerable potential use for preliminary visual and semi-automated landslide inventorying as an important supplement to field mapping.

Keywords Post-disaster · Landslide inventory · Remote sensing · VHR-HR satellite image · Rainfall · Serbia

Introduction

A massive low-pressure cyclone, "Tamara", hit the Western Balkan countries in May 2014, resulting in extensive flooding and landslide damages in Serbia and Bosnia and Herzegovina. The floods, flash floods and landslides resulted in 51 casualties, approximately 32,000 people being evacuated and more than 1.6 million people being directly or indirectly affected in Serbia alone. The Serbian government declared a state of emergency covering the whole territory of Serbia on May 15, 2014. The United Nations Disaster Assessment and Coordination Team (UNDAC) assisted immediately and estimated that roughly more than 2000 landslides were activated in the western and central parts of Serbia (UNDAC 2014). Some of the locations in western Serbia were affected by many flow-type landslides, which had never previously been reported in these areas. These landslides caused severe damage to the local municipalities (residential areas, roads, infrastructure facilities, cultivated lands, pastures and forests), as well as to the highly urbanized areas in the city of Belgrade, the capital of Serbia. In the framework of the post-disaster recovery led by the United Nations Development Programme (UNDP) Office in Serbia, several actions were taken with the aim of supporting landslide risk assessment and management in the affected municipalities. Following these activities, attention was focused on developing a fast and efficient methodology for a post-event landslide inventory, which had to be completed within 5 months for more than 14,500 km², with limited financial resources and personnel. It entailed integrating and homogenizing all of the landslide data in the National Landslide Database, which is yet to be completed.

Many recent studies have highlighted the importance of using remote sensing technologies for fast landslide mapping in similar situations (Tralli et al. 2005; Lin et al. 2011; Joyce et al. 2014; Kwan and Ransberger 2010; Guzzetti et al. 2012; Lira et al. 2013; Bhambri et al. 2016; Martha et al. 2015; Ray et al. 2016). In particular, during the response and recovery phases of the disaster and crisis cycle, only very fast delivery of up-to-date, accurate and comprehensive image analysis products can significantly assist in the assessment of large-scale disaster damage (Voigt et al. 2007; Denis et al. 2016). Event-based inventories are important for documenting the full extent of a landslide disaster caused by rainfall (Bucknam et al. 2001; Guzzetti et al. 2004; Cardinali et al. 2006; Lin et al. 2011; Marjanović and Abolmasov 2015) or earthquakes (Sato et al. 2007; Sato and Harp 2009; Tang et al. 2015; Yang and Chen 2010; Xu et al., 2014; Martha et al. 2016; Shafique et al. 2016) and for damage assessment related to post-disaster management activities (Martha and Kumar 2013; Ciampalini et al. 2015). Landslide event-based inventory maps in the post-disaster phase are usually created through the interpretation of stereoscopic aerial photographs taken after the event (Bucknam et al. 2001; Guzzetti et al. 2004, Tang et al. 2015) using visual (Marjanović et al. 2016, Lin et al. 2011) or semi-automatic analysis (Martha et al. 2010, 2012; Mondini et al. 2011) of the multispectral and multitemporal satellite images, using high resolution digital elevation model analysis (Chen et al. 2006; Booth et al. 2009; Kwan and Ransberger 2010; Iwahashi et al. 2012), using extensive field surveys (Cardinali

et al. 2006; Marjanović and Abolmasov 2015) or using a combination of these techniques (Mondini et al. 2011; Xu et al. 2013, Murillo-García et al. 2015; Alkevli and Ercanoglu 2011). In relation to all the abovementioned case studies, this case study differs in some respects. Firstly, the regional extent of similar studies is much smaller than the one considered here (Lin et al. 2011, Martha and Kumar 2013), except for the earthquake-induced landslide cases (Tang et al. 2015; Martha et al. 2016). This finding implies that very high resolution (VHR) image coverage of sufficient quality was difficult to obtain for the entire area of interest, as highlighted in Xu et al. (2014). Secondly, previous case studies combined the same resolution of pre-event and post-event (VHR or high resolution (HR)) images for visual (Martha et al. 2015; Lira et al. 2013) or VHR satellite data for semi-automatic recognition (Martha and Kumar 2013). Although highly recommended, this is a demanding and expensive approach for large areas, such as the one in this case study. Instead, it is herein proposed that only some parts of the whole area should have VHR coverage, and these should be used for control of the semi-automated landslide mapping, performed by using lower resolution images. Thereby, semi-automated mapping can be extrapolated outside the VHR coverage. The pilot area in the Krupanj municipality was herein used to explore this option.

The main objective of this research was an analysis of the available multiresolution satellite image data for a fast post-event landslide inventory of the 23 municipalities affected by the extreme rainfall event during May 2014. VHR and HR Pléiades, SPOT 6 and WorldView-2 (WV2) multispectral satellite images were used for visual landslide recognition and to build an inventory to support an extensive landslide mapping field campaign. The VHR and HR satellite images covered a 9167.11-km² territory, and a total of 1298 landslides of various types were visually recognized in these images. Additionally, the free-to-access HR Landsat 8 multitemporal satellite images and open source QGIS software were used for the analysis of the Krupanj municipality (341 km²) as a test area for the semi-automatic recognition of landslide occurrences. The objective of this additional analysis was to show that the semi-automatic landslide recognition in HR satellite images could be a useful tool for other affected territories where VHR satellite images are unavailable. In addition, another objective was to show how a preliminary landslide inventory obtained by remote sensing analysis can be an essential support for a field campaign, as well as a reliable source for landslide inventorying in inaccessible terrains. An event-based landslide inventory for a particular rainfall trigger event was undertaken for the first time on a previously unheard of scale in Serbia. Additionally, for the first time, the entire database has been made publicly available via an interactive web portal (http://geoliss.mre.gov.rs/beware/).

Study area
The study area covered 11.840 km², i.e. 23 of the 27 municipalities included in the UNDP post-disaster BEWARE Project activities in the western and central parts of the Republic of Serbia (Fig. 1). Four municipalities were excluded from the analysis

because there were no landslides that occurred during the May 2014 rainfall event, only floods and flash floods. In the 23 municipalities that were included, the total population was approximately 1,000,000 people. It is also important to mention that the majority of these municipalities are characterized as underdeveloped and undeveloped (11 underdeveloped and 4 undeveloped of the 23 chosen municipalities), with fragile economies, poor industrial potentials and high unemployment rates (http://www.regionalnirazvoj.gov.rs/ data from 2014, accessed January 2017). All these factors make these areas even more vulnerable to disastrous landslide events, such as the ones that occurred in May 2014.

Geological settings
The geological and geomorphological settings and other environmental conditions are very complex. The central and western parts of Serbia are situated in the region of the so-called Dinaric fold-and-thrust belt, encompassing several continental and oceanic tectonic units that were left behind after the extensive processes of the Jurassic closure of the Neotethys Ocean (Schmid et al. 2008) and the Cretaceous–Oligocene nappe stacking (Schefer 2010; Ustaszewski et al. 2010; Mladenović et al. 2015). The oceanic tectonic units show a typical sequence of peridotite, gabbro and basalt covered by an ophiolitic mélange (Dimitrijević 1997). The continental units are mostly composed of slightly metamorphosed sandstones and shales covered by shallow limestone sequences (Dimitrijević 1997). All the tectonic units are covered by Cretaceous flysch deposits. During the Miocene, this area was affected by an extension, which provided the conditions leading to smaller basins in the so-called Dinaric Lake system (Krstić et al. 2003). These basins are mostly filled with limestones, sandstones, marls and shales (Dimitrijević 1997).

The geomorphological settings are mostly characterized by the fluvial and fluvial-denudation features that are dominant in western and central Serbia. Erosional features prevail on the slopes of the hills and mountains, while depositional features occupy basins, valleys and other depressions. These deposits are mainly within the clay fraction and are hence considered to be responsible for the development of the most common types of landslides in this region (Menković et al. 2003; Mihalić Arbanas et al. 2013; Abolmasov et al. 2015). However, the landslides in Serbia, with all their diverse mechanisms and types of mobilized material (Cruden and Varnes 1996; Cruden and VanDine 2013; Hungr et al. 2014), involve many other factors, such as the local geomorphological characteristics, engineering geological material properties, degree and depth of the weathering substratum, land cover and land use as well as the characteristics of the factors that trigger them (e.g. the unusually high precipitation rate in May 2014).

The municipality of Krupanj, one of the most affected areas in May 2014, was selected as a test site for more detailed research. This area is located in western Serbia and covers 341 km², with a population of 17,295 inhabitants (Fig. 1). The majority of the territory consists of Devonian-Carboniferous weathered low-crystalline metamorphic rocks, including mud
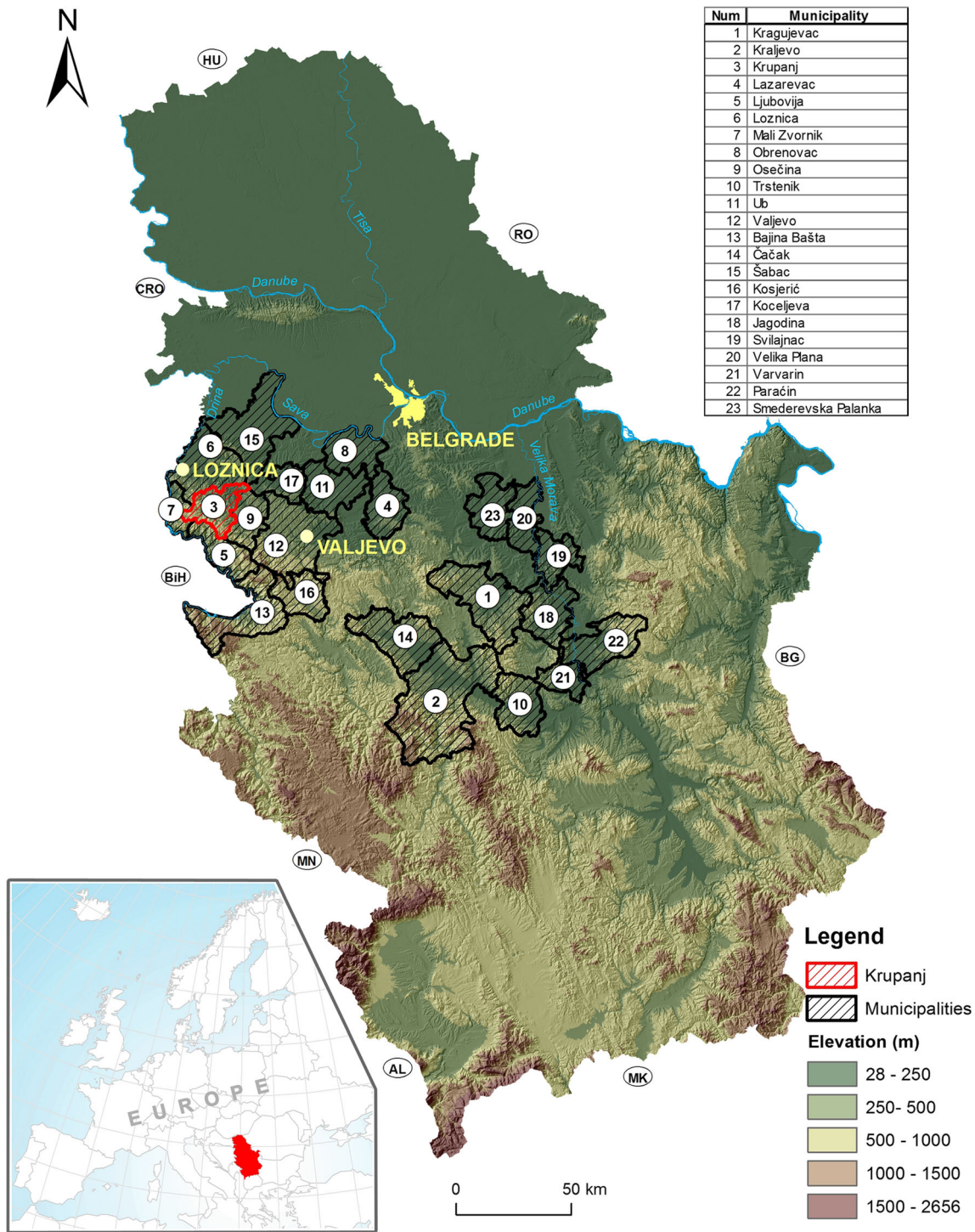
Num	Municipality
1	Kragujevac
2	Kraljevo
3	Krupanj
4	Lazarevac
5	Ljubovija
6	Loznica
7	Mali Zvornik
8	Obrenovac
9	Osečina
10	Trstenik
11	Ub
12	Valjevo
13	Bajina Bašta
14	Čačak
15	Šabac
16	Kosjerić
17	Koceljeva
18	Jagodina
19	Svilajnac
20	Velika Plana
21	Varvarin
22	Paraćin
23	Smederevska Palanka

Legend

Krupanj

Municipalities

Elevation (m)

28 - 250

250- 500

500 - 1000

1000 - 1500

1500 - 2656

Fig. 1 Geographical position of the Republic of Serbia and the position of the included municipalities in the research

and clay shales, phyllites and argillaceous schist (approximately 80%). Permian meta-sediments (clay shales, sandstone and flysch), Triassic limestone and sandstone and Cretaceous limestone make up the remaining 20% of the territory. The weathering zone thickness in these rocks is between 1 to 5 m, depending on the dominant lithological units and structures. Quaternary deposits are generally represented by alluvial and diluvial sediments. The topography is a typical low
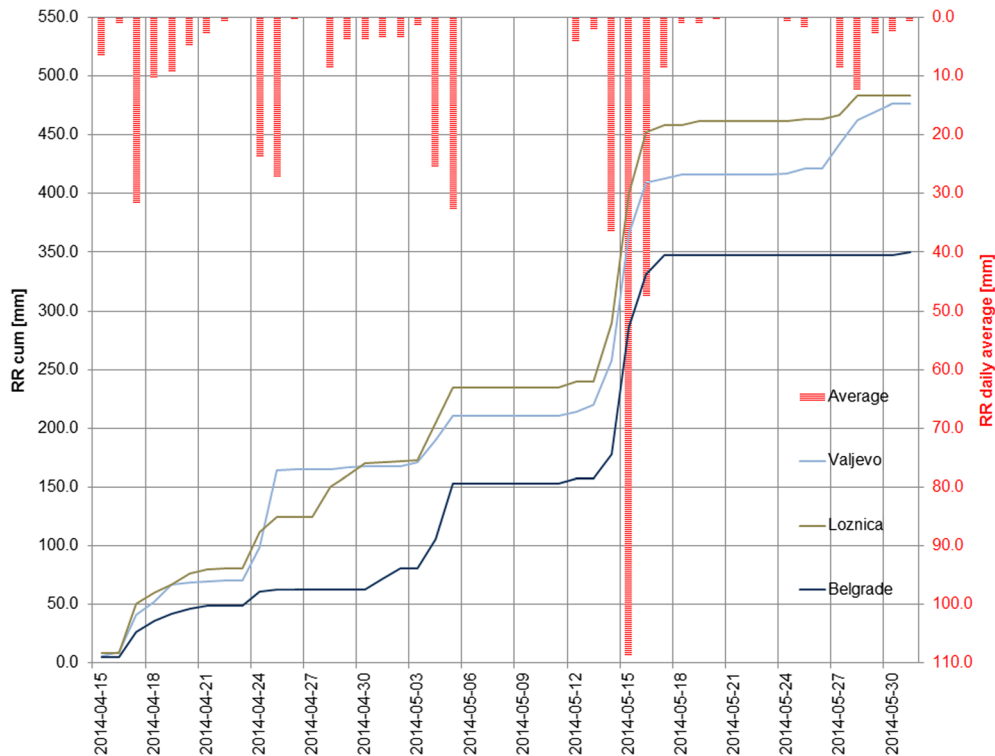
Fig. 2 Antecedent rainfall, from April 15 to May 13, 2014 for Belgrade, Loznica and Valjevo meteorological stations

mountainous to hilly relief landscape with predominantly gentle to moderate slopes (7–21°) and many micro-relief forms enclosed in relatively small catchments.

Rainfall event

In the third week of May 2014, the massive low-pressure cyclone Tamara swept through the Western Balkans, resulting in extreme precipitation over a short period, which caused floods, flash floods and massive landslides in the western and central parts of Serbia. The highest 48-h rainfall was registered at the Loznica Main Meteorological Station (MMS) in the western part of Serbia, exceeding 160 mm/48 h, which corresponds to an extreme rainfall that statistically occurs once every 1000 years over that area (1000-year return period). MMS in Valjevo and Belgrade recorded precipitation of a 400-year return period for the same duration (Prohaska et al. 2014). The highest values of 72-h rainfall were also recorded in Loznica (213 mm), Valjevo (190 mm) and Belgrade (174 mm). The following flood events and landslides were triggered instantly, but it is possible that the massive landslides were also initiated by the antecedent rainfall, which was unusually high from April 15 to May 13, 2014 (Fig. 2), when the monthly precipitation exceeded half of the previous annual average. Namely, the annual precipitation averages for the Loznica, Valjevo and Belgrade MMSs were 868, 788 and 691 mm/year, respectively (reference period, 1981–2010). Even though these values are seemingly low in comparison to other latitudes (e.g.

tropical or Mediterranean scenarios), 48–72-h rainfall of approximately 100–200 mm (10–20% of annual total) at these three MMS represents an extreme level of soil saturation, especially when coupled with the antecedent cumulative rainfall effects (causing constant, gradual deterioration of the soil strength by decreasing the effective stresses).

Materials and methods

Data sources

The main input sets for the visual analysis were all available in the cloud-free (less than 5% cloud) and snow-cover-free series of the VHR and HR images from May 23, 2014 to November 04, 2014, provided by the UNDP Office in Serbia through the post-disaster BEWARE Project. The general characteristics of the available satellite images, including their date of acquisition, resolution, number of scenes and name of the mission, are given in Table 1. The VHR and HR satellite images covered 9167.11 km² or 77.43% of the study area (Table 2 and Fig. 3). For two of the municipalities (Paraćin and Smederevska Palanka), there were no available satellite images (i.e. 23.57% of study area) (Table 2). Pléiades VHR images covered only 19.52% of the study area, while the rest was covered by the HR SPOT 6 and WV2 missions (38.57 and 19.33% of the study area, respectively) during the required time spans (Table 2).

Multitemporal, pre-event (August 9, 2013) and post-event (August 19, 2014) free access Landsat 8 satellite images, number 187/29

Table 1 Post-disaster VHR and HR satellite data used for visual analysis

Mission	Sensor type	Spectral bands (µm)	Original resolution (m)	Resolution after processing (m)	Acquisition date	Number of scenes
Pléiades	MS	B (0.43–0.556)	2	0.5	2014-05-21	1
		G (0.49–0.61)			2014-06-08	1
		R (0.60–0.72)			2014-06-29	1
					2014-10-08	2
	PAN	Pan.(0.48–0.83)	0.5		2014-10-09	1
					2014-11-04	1
SPOT 6	MS	B (0.455–0.525)	6	6	2014-05-21	1
		G (0.53–0.59)				
		R (0.625–0.695)				
		IR (0.760–0.890)				
	PAN	Pan.(0.45–0.745)	1.5	1.5	2014-09-19	1
WorldView-2	MS	B (0.45–0.51)	1.5	1.5	2014-05-24	4
		G (0.51–0.58)			2014-07-04	
		R (0.63–0.96)				
	PAN	Pan. (0.45–0.9)	1.5	1.5	2014-05-23	5
					2014-06-30	
Landsat 8	MS	UB (0.43–0.45)	30	15	2013-08-09	1
		B (0.45–0.51)				
		G (0.53–0.59)				
		R (0.64–0.67)				
		NIR (0.85–0.88)				
		SWIR1 (0.85–0.88)				
		SWIR2 (2.11–2.29)				
		CIR (1.36–1.38)				
		TIRS1 (10.60–11.19)				
		TIRS2 (11.50–12.51)				
	PAN	Pan. (0.50–0.68)	15		2014-08-19	1

(row/path), were analysed for the Krupanj municipality as a test of semi-automatic landslide recognition. These images were also cloud-free, and they had similar vegetation and agricultural conditions. The territory of Krupanj, as indicated earlier, was chosen not only because it provided a diversity and multiplicity of landslide examples but also because it had large coverage in the VHR Pléiades images (87.33% of the territory) (Table 2).

Data processing
The Pléiades, SPOT 6 and WorldView-2 images used in the visual analysis were orthorectified and georeferenced by the vendor. The images have been pan-sharpened and mosaicked. The visual recognition was aided by a 25-m shaded relief derived from the DEM (supplied by the Republic Geodetic Authority of Republic of Serbia) using different transparency settings, as well as a pre-event background image from the Google platform. In all multispectral images, the usual true RGB colour composite and false colour composite were used (Fig. 4).

Data pre-processing and Landsat 8 image processing (Fig. 5) were performed in the open source QGIS software. To maximize the usefulness of the data, radiometric calibration and

Table 2 List of municipalities and spatial coverage of municipality areas by VHR and HR satellite data

No.	Municipality	Municipality area (km²)	Coverage of municipality area (km²)			Coverage of municipality area (%)		
			Pléiades	SPOT 6	WV 2	Pléiades	SPOT 6	WV 2
1	Kragujevac	833.94	293.21	–	388.92	35.16	0.00	46.64
2	Kraljevo	1528.7	268.73	–	–	17.58	0.00	0.00
3	Krupanj	341.65	298.36	314.65	–	87.33	92.10	0.00
4	Lazarevac	383.3	322.31	187.65	–	84.09	48.96	0.00
5	Ljubovija	355.67	46.43	355.67	163.51	13.05	100.00	45.97
6	Loznica	609.63	81.66	609.63	–	13.40	100.00	0.00
7	M. Zvornik	183.43	17.42	183.43	–	9.50	100.00	0.00
8	Obrenovac	409.89	188.63	–	–	46.02	0.00	0.00
9	Osečina	318.4	13.03	318.4	–	4.09	100.00	0.00
10	Trstenik	447.83	96.81	–	313.2	21.62	0.00	69.94
11	Ub	456.36	235.97	27.67	–	51.71	6.06	0.00
12	Valjevo	903.64	33.99	899.6	–	3.76	99.55	0.00
13	B. Bašta	668.6	350.89	363.76	295.73	52.48	54.41	44.23
14	Čačak	635.86	63.89	306.08	–	10.05	48.14	0.00
15	Šabac	796.89	–	391.89	–	0.00	49.18	0.00
16	Kosjerić	358.42	–	358.41	–	0.00	100.00	0.00
17	Koceljeva	257.29	–	250.12	–	0.00	97.21	0.00
18	Jagodina	468.7	–	–	254.71	0.00	0.00	54.34
19	Svilajnac	325.9	–	–	316.4	0.00	0.00	97.08
20	V. Plana	344.89	–	–	335.02	0.00	0.00	97.14
21	Varvarin	249.2	–	–	221.33	0.00	0.00	88.82
22	Paraćin	540.38	–	–	–	0.00	0.00	0.00
23	S. Palanka	421.02	–	–	–	0.00	0.00	0.00
Total area (km²)		11,839.59	2311.33	4566.96	2288.82			

correction procedures were applied (Chavez 1996). Pre-processing included radiometric calibration and atmospheric correction; the derived data were extracted for the surface temperature calculation (Moran et al. 1992; Valor and Caselles 1996; Jiménez-Muñoz et al. 2006; Osiñska-Skotak 2007). The surface temperature is generated using a Split Window algorithm, which includes the emissivity, vapour, temperature profiles, transmittance and reflection (Fig. 5). Pre-processing further included brightness optimization, pan-sharpening and masking procedures (defining the areas covered by clouds and their removal). Processing included Principal Component Analysis (PCA) and semi-automatic classification. PCA was conducted on six pre-processed multispectral bands (from two to seven), and PCA2 was the one that best showed the landslides because PCA2 gives the relationship between bands 5 and 3 (red and infrared), which represents the Vegetation Index. A raster calculator (Change detection) was used to compute the difference between the pre- and post-event PCA2s to compare the differences in their vegetation cover and, thereby, the potential presence of slides and flows. A supervised classification of land cover was completed using a semi-automatic classification plug-

in with a Minimum Distance algorithm using four classes (Minu and Bindhu 2016), which will be explained in "Data analysis" section.

Data analysis

Visual analysis and interpretation

Visual analysis and interpretation were performed on the available Pléiades, SPOT 6 and WorldView-2 satellite images provided by UNDP. Originally, the high- to low-resolution (1.5–6 m) multispectral and panchromatic SPOT 6 and WorldView-2 satellite images and their acquisition dates had limited usefulness (Table 1) because their visual interpretation was time consuming and constrained only to large slides, according to Metternich and Hurni (2005). On the other hand, the VHR Pléiades images (0.5 m) were very helpful for fast detection and interpretation of all landslides types. The landslides in these images were detected on the basis of a set of standard criteria: their tone changes and the morphological footprints in the relief. Tone changes (for black-and-white images) or changes in colour (colour images) indicated
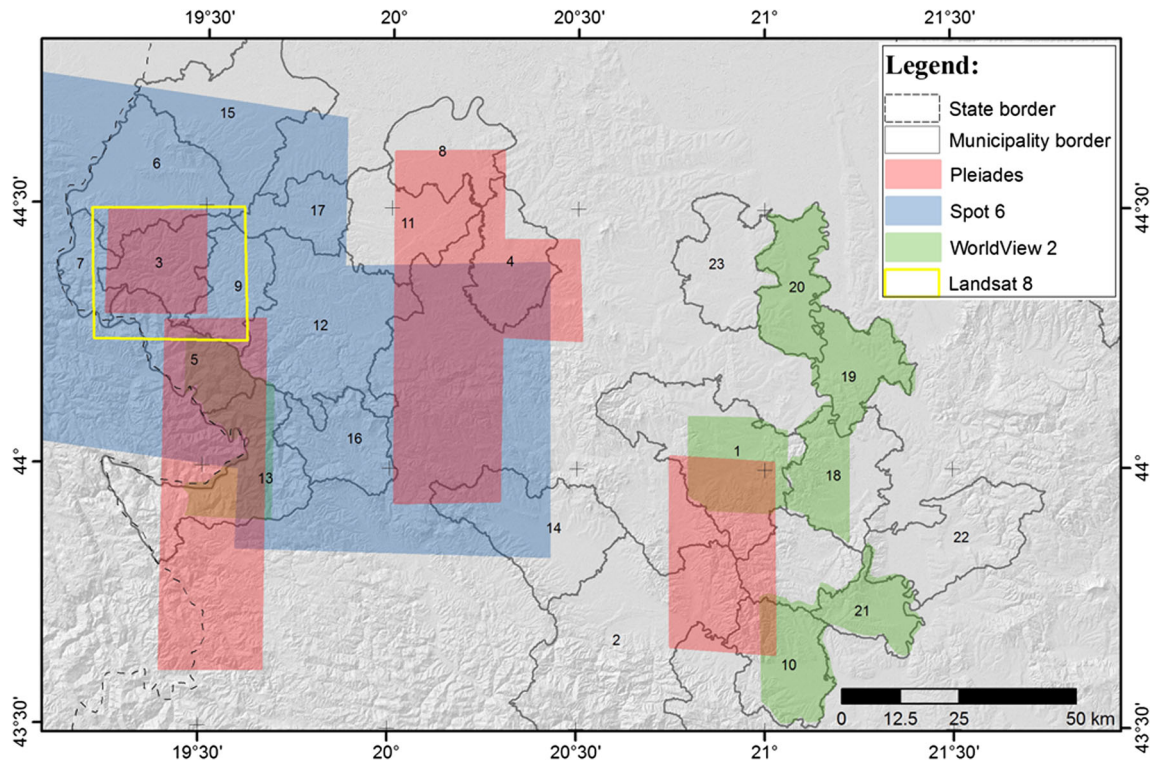
Fig. 3 Spatial coverage of municipality areas by satellite data used in the analysis (list of municipalities is given in Table 2)

a change in soil moisture. Visual interpretation allowed a relatively confident discerning of flows, as elongated irregular forms developed down the slope and shallow slides in irregular elliptical forms (Figs. 6 and 7). Some of the flows followed the existing local micro-relief depressions on the slopes, but others were formed in the gullies of the upstream zones. Flash flood zones were also routinely digitized (Fig. 8).

All landslide occurrences were interpreted with a specified degree of certainty. The level of certainty was determined based on the number of satisfied interpretation criteria, such as the morphological footprints in the relief, tone/colour changes, soil moisture changes, gullies, vegetation, textures (including cracks), surface disturbances and artificial object disturbances (Haugerud et al. 2003; Schulz 2007). Independent of the

landslide size, if the phenomenon satisfied all six of these criteria, the highest level of certainty was assigned to it. The highest level of certainty was labelled "1" (890 landslides), medium was labelled "2" (214 landslides, which satisfied a minimum 3/6 criteria), while the lowest level of certainty was marked "3" (179 landslides); see the example in Fig. 9. Approximately 516 of the 890 landslides with the highest interpretation certainty were flow-type landslides, suggesting that this type of mechanism provides the easiest and most reliable interpretation. In contrast, approximately 100 of the 179 occurrences with the lowest interpretation certainties belonged to slide-type landslides, suggesting that this type has the least reliable interpretation variants. Since 70% of all of the interpreted instabilities fell in the "1" category, where all criteria for interpretation were
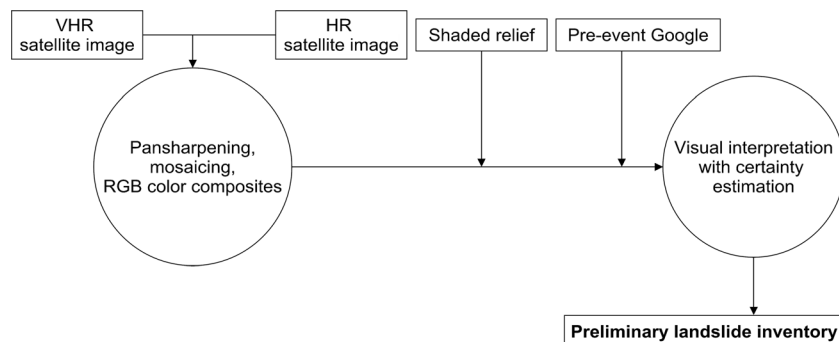

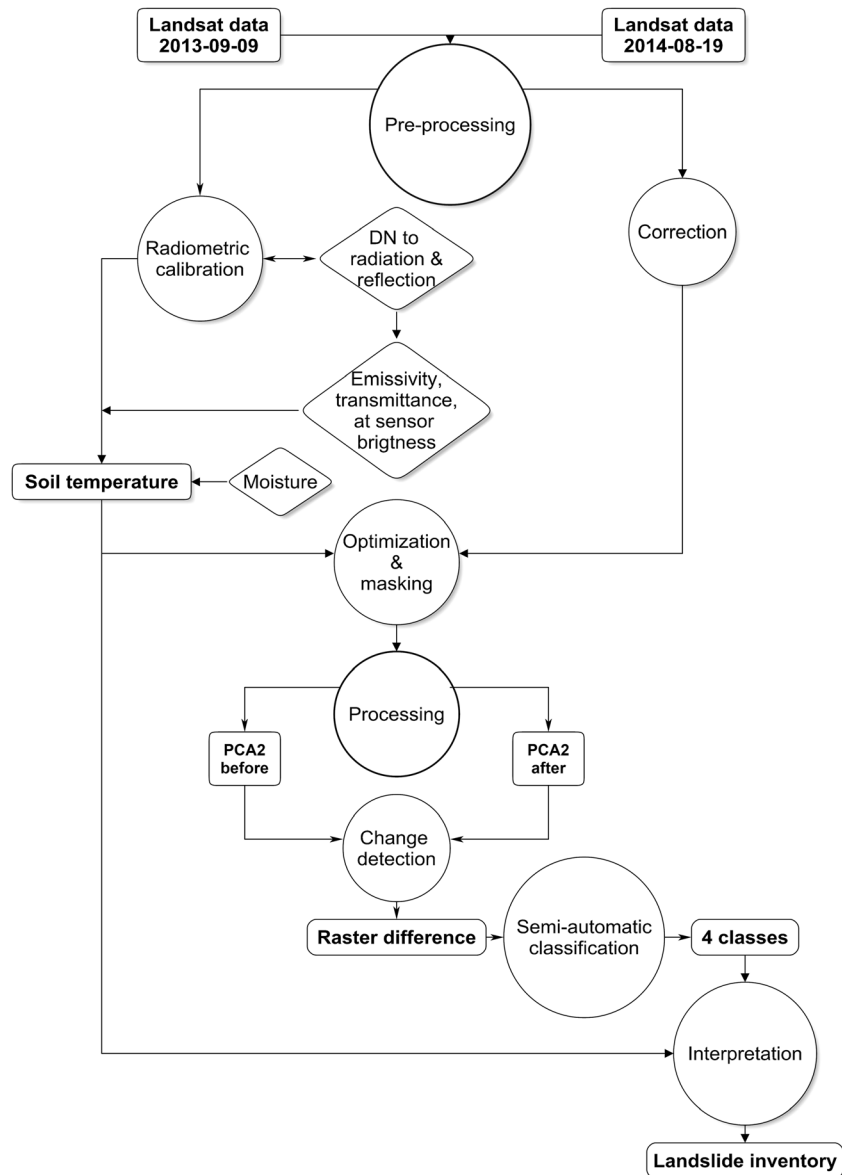**Fig. 4** Flow chart of visual landslide recognition

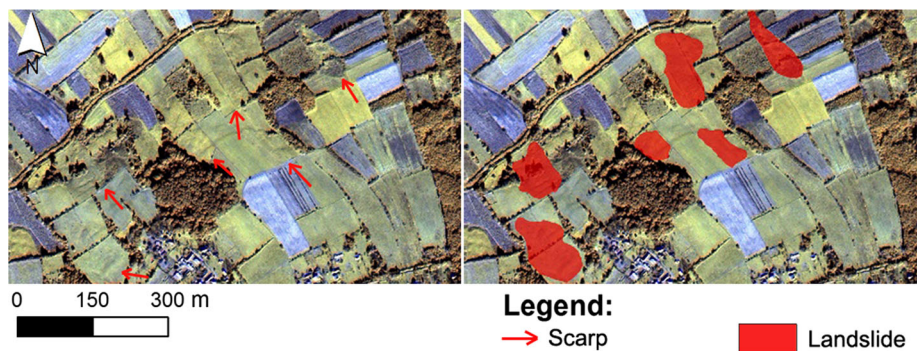**Fig. 5** Flow chart of applied pre-processing and processing procedures for semi-automatic landslide recognition

Fig. 6 *Left*: Pléiades satellite image (resolution 0.5 m, RGB 3, 2, 1). *Right*: Recognition of landslides, Krupanj municipality
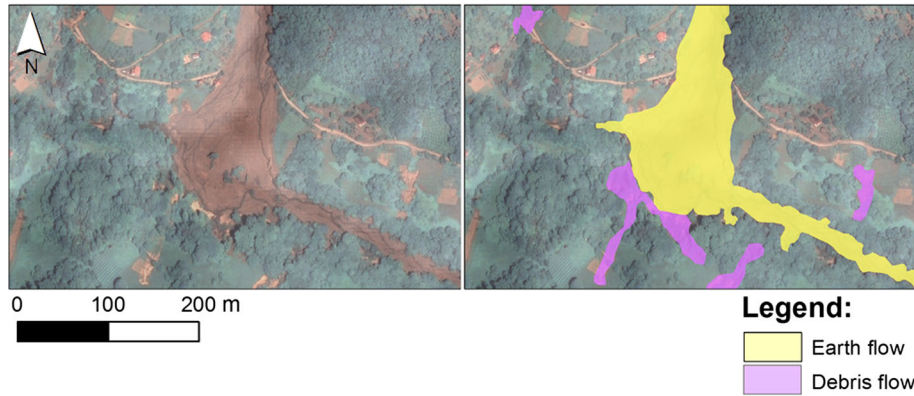
Fig. 7 *Left*: Pléiades satellite image (resolution 0.5 m, RGB 3, 2, 1). *Right*: Recognition of earth flow (*yellow*) and debris flows (*pink*), Krupanj municipality

satisfied, it is already clear that VHR-HR images provide an efficient and reliable source of information.

Semi-automatic detection of landslides for the test area

The spectral plot, original bands and soil temperature intermediate products described in "Data processing" section were analysed with a semi-automatic supervised classification in order to determine the target classes. The following classes were selected: areas that included clouds and/or shadows—class 0; areas of cultivated land—class 1; areas under water and vegetation—class 2; and areas with bare land (eroded areas)—3 (Fig. 10). The process of automatic classification misclassified alluvial plains and river terraces as eroded areas (that potentially contain landslides); therefore, they were manually removed from class 3. It was found that instabilities that represent a single body were disaggregated into multiple polygons. All such cases were identified and merged into logical entities in class 3. A semi-automatic classification of the PCA2 difference (PCA/before and PCA/after) (Krupanj) singled out more than 4500 occurrences of instabilities in the test area. The obtained polygons were plotted and correlated with a slope map derived from the digital elevation model (25 × 25 m). According to the morphological parameters in the test area (the Krupanj municipality), it was assumed that slopes ranging between 5° and 25° were possible hosts of landslides according to field data and statistical analysis of slope angle range vs.

landslides (the average slope angle for all landslides is 23°). All zones outside of this range were excluded from further semi-automatic analysis for simplification, and the number of total polygons was reduced. Many of these were split polygons that belonged to the same landslide and had to be aggregated into single logical entities. The remaining split polygons were visually/manually grouped into logical entities.

Results and discussion

Results of the analysis of the whole study area

The resolutions of the satellite images that covered the whole research area and included all 23 municipalities varied from 0.5 m for the Pléiades images to 1.5–6 m for the SPOT 6 and WV2 images. This variance was the source of the uneven interpretation qualities and different numbers of recognized landslides throughout the area. The field mapping campaigns, on the other hand, had lesser but more consistent areal coverage (Table 3).

Based on the visual interpretation and analysis of the VHR and HR satellite images of the study area, a total of 1298 landslides (592 slides and 691 debris/earth flows) were recognized, while 15 instances of movements were not assigned to be slide- or flow-type movements since they represent complex types of movement. The total number of visually recognized landslides per municipality included in the research is given in
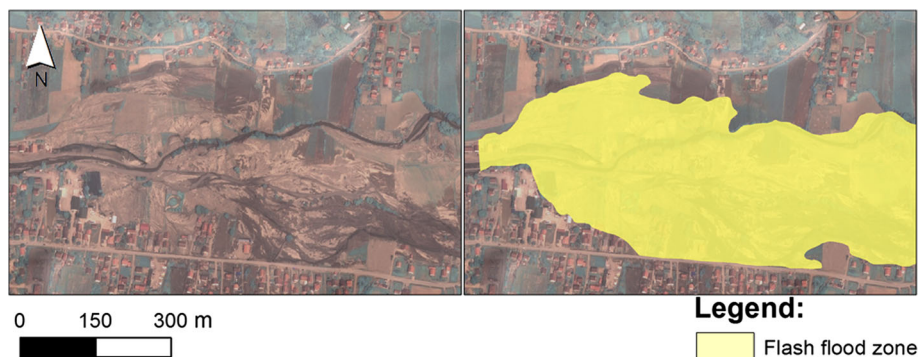

Fig. 8 *Left*: Pléiades satellite image (resolution 0.5 m, RGB 3, 2, 1). *Right*: Recognition of flash flood zone Krupanj municipality urban area
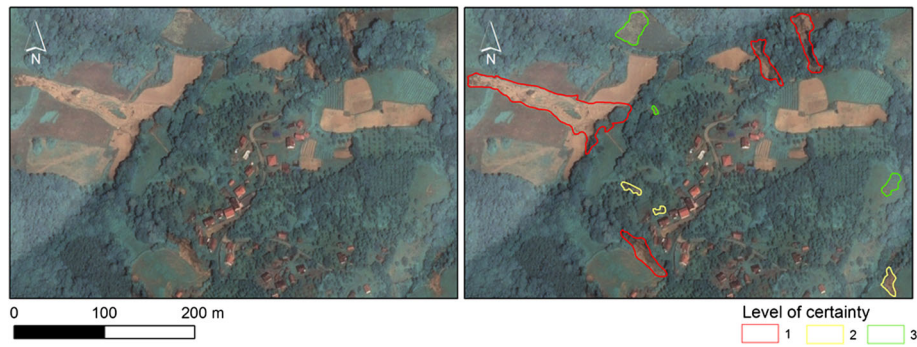
Fig. 9 *Left*: Pléiades satellite image (resolution 0.5 m, RGB 3, 2, 1). *Right*: Illustration of different level of certainty of landslide (*red polygon* certainty 1, *yellow polygon* certainty 2, *green polygon* certainty 3)

Table 3. Several municipalities were covered by the relatively low-resolution SPOT 6 and WorldView-2 (MS) satellite images, or they were not covered by any satellite images at all. In these municipalities, subsequent field work has only established slides. Because it is relatively difficult to identify slides with relatively small displacements (below 12 m) and small magnitudes (below 500 m²) without stereo images and considering the resolution of the available satellite images in the territory of these municipalities, it has not been possible to visually interpret slides.

The largest landslide/debris flow was recognized in the municipality of Ljubovija, near the village of Selanac, with an area of 85,222.23 m² (Table 4). This landslide/debris flow was 1.5 km long and, at its wider part, was 220 m wide (Figs. 11 and 12).

Results of the analysis of the test area (Krupanj municipality)
Results of the visual interpretation of the satellite images in the Krupanj test area are shown in Fig. 13. A total of 507

landslides (Table 5) were assigned certainty labels of "1" and "2".

A semi-automatic analysis was applied in order to highlight the differences in the relief for the period after a heavy rainfall by comparing the pre-event and post-event images (Fig. 14). The red/orange colour represents a deficit of mass, while the blue colour represents a surplus of mass (accumulation of transported material). Since the resolution of the Landsat 8 images was 30 m, only instabilities longer/wider than 30 m were recognized. White zones in the image represent a mask for clouds and shadows. These results were burdened with undesired interferences, such as alluvial fans and agricultural zones, which were shown as surplus/deficit masses. Given the spectral signature of the target classes (Fig. 10), the minimum distance algorithm had difficulties coping with the classifications in spectral overlap domains, especially for cultivated land, vegetation and bare land.

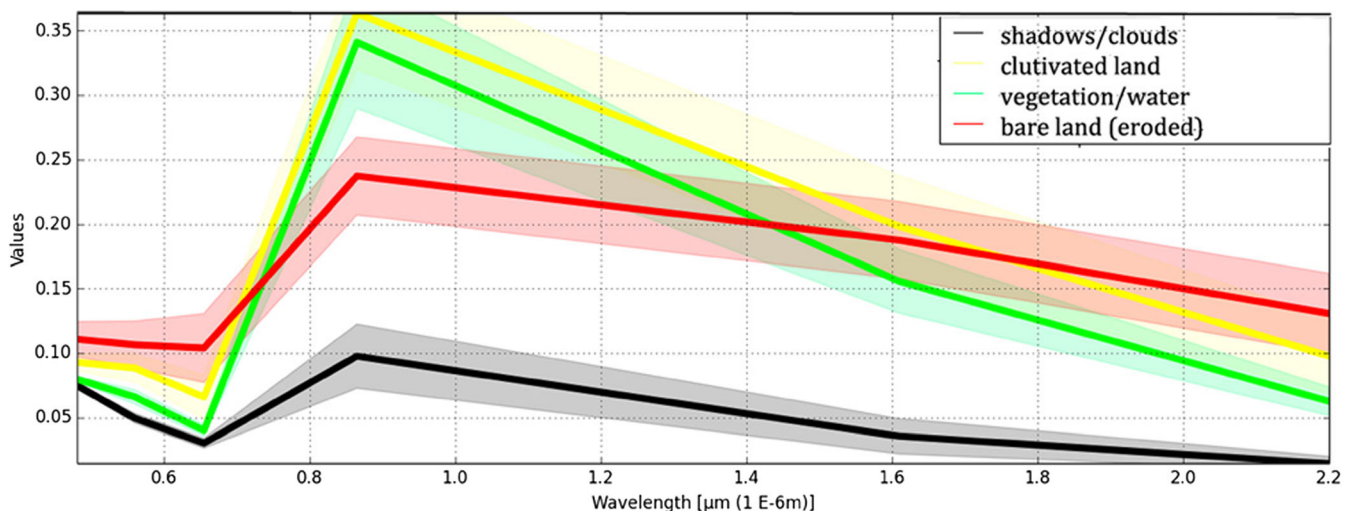As a result of the semi-automatic classification and reclassification (explained in "Semi-automatic detection of

Fig. 10 Diagram of wavelength for different classes

Table 3 List of visually recognized landslides per municipality

No.	Municipality	Total number of landslides (all type) Satellite image data				Field campaign data Slides and flows
		Slides	Debris/earth flows	Complex	Total	
1	Kragujevac	25	27		52	155
2	Kraljevo	28	23		51	188
3	Krupanj	220	277	10	507	160
4	Lazarevac	62	18		80	36
5	Ljubovija	96	104	3	203	66
6	Loznica	5	18	2	25	108
7	M. Zvornik	34	59		93	26
8	Obrenovac	23	3		26	15
9	Osečina		1		1	210
10	Trstenik	2	2		4	66
11	Ub	7	14		21	26
12	Valjevo[a]					222
13	B. Bašta	75	143		218	144
14	Čačak[a]					126
15	Šabac[a]					42
16	Kosjerić[a]					62
17	Koceljeva[a]					55
18	Jagodina[a]					9
19	Svilajnac[a]					27
20	V. Plana[a]					1
21	Varvarin	15	2		17	7
22	Paraćin[a]					26
23	S. Palanka[a]					8
Total		592	691	15	1298	1785

[a] Municipalities without VHR image coverage (less than 10%)

Table 4 Details of visually recognized landslides per municipality

| No.	Municipality	No. of landslides	Landslide metric parameters			
			Min size (m^2)	Max size (m^2)	Average size (m^2)	Total area (m^2)
1	Kragujevac	52	194.90	11,014.58	1607.06	83,567.02
2	Kraljevo	51	146.00	19,874.6	1952.43	103,479.24
3	Krupanj	507	68.60	17,137.5	1862.36	938,630.30
4	Lazarevac	80	168.64	8010.57	2056.06	164,484.43
5	Ljubovija	203	93.19	85,222.23	1886.50	377,300.00
6	Loznica	25	164.19	13,650.16	2946.36	91,337.16
7	M. Zvornik	93	113.22	10,388.12	1540.58	124,787.20
8	Obrenovac	26	152.46	12,437.35	3143.44	81,729.52
9	Osečina	1	2665.12	2665.12	2665.12	2665.12
10	Trstenik	4	816.57	8935.02	3418.02	13,672.10
11	Ub	21	263.66	10,180.63	2445.30	51,351.33
13	B. Bašta	218	62.40	8218.70	1026.10	230,868.80
21	Varvarin	17	596.61	8409.48	2866.90	48,738.88
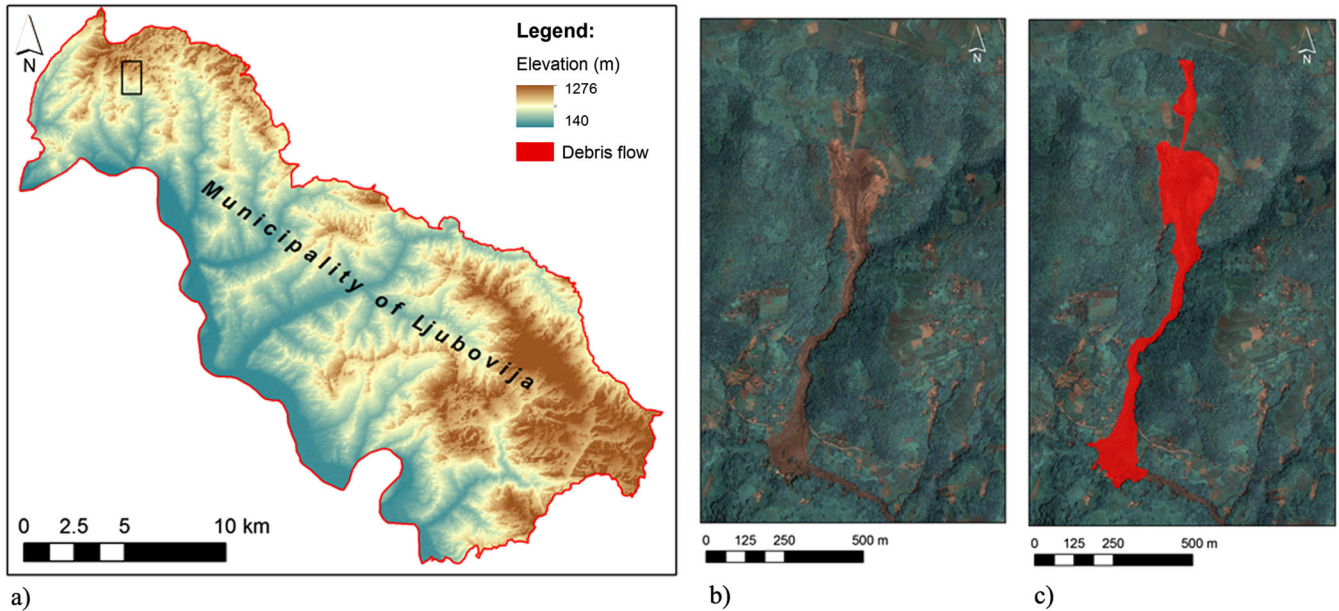
Fig. 11 Example of a representative visually recognized Selanac landslide/debris flow

landslides for the test area" section), 490 instances of mass differences were identified. Those polygons were interpreted as landslides without a more precise determination of the mechanism of transport (slides/flows). After their interpretation, it was concluded that most of the identified instances were positioned on slopes with values of approximately 20° and were close to or within gullies.

The total number of recognized landslides in the Krupanj municipality based on the different source data and applied methodology of inventorying is shown in Table 5.

The visual satellite image analysis, supervised classifications and field observations were cross-compared (Fig. 15). Since the lowest common resolution for these three sources was 30 m (Landsat 8 image resolution), only landslides larger than 900 m² in the area were considered. The field data were loosely considered to be the ground truth but were mostly used as a reference. The reason for this lies in the fact that the flows were recognized with much higher certainty in the satellite images than the slides (i.e. flows were preferred via

image analysis), while one of the focuses of the field work was mapping of slides or other types that could not be clearly identified from satellite images (i.e. slides were preferred via field work). The cross-comparison for Krupanj shows some matching between the visual interpretation and the ground truth, i.e. an approximately 26% match, especially for the larger slides. A similar match of approximately 20% was noted between the semi-automatic analysis and ground truth. A cross-comparison between the visual and semi-automatic analyses gives a better match, with an overlap of 41% for larger slides.

Considering the number of identified instabilities and the resolution of the available data, the visual interpretation provided reliable results, especially for the mapping of inaccessible flows. Field data (160 landslides and debris/earth flows) cover only accessible terrain, which is the reason behind the relatively small number of detected instabilities in this dataset compared to the number found via the remote sensing method (507 landslides and flows). The second reason was that the
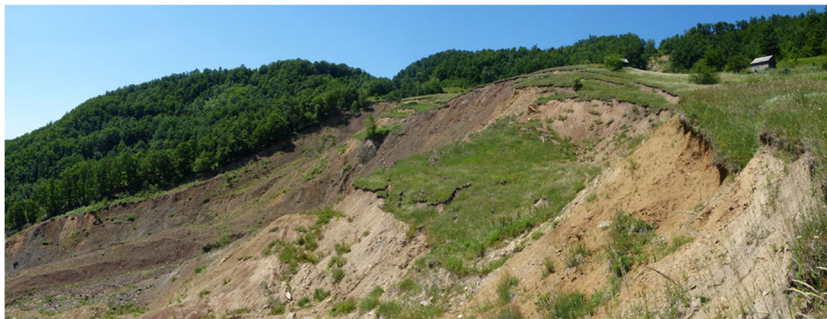

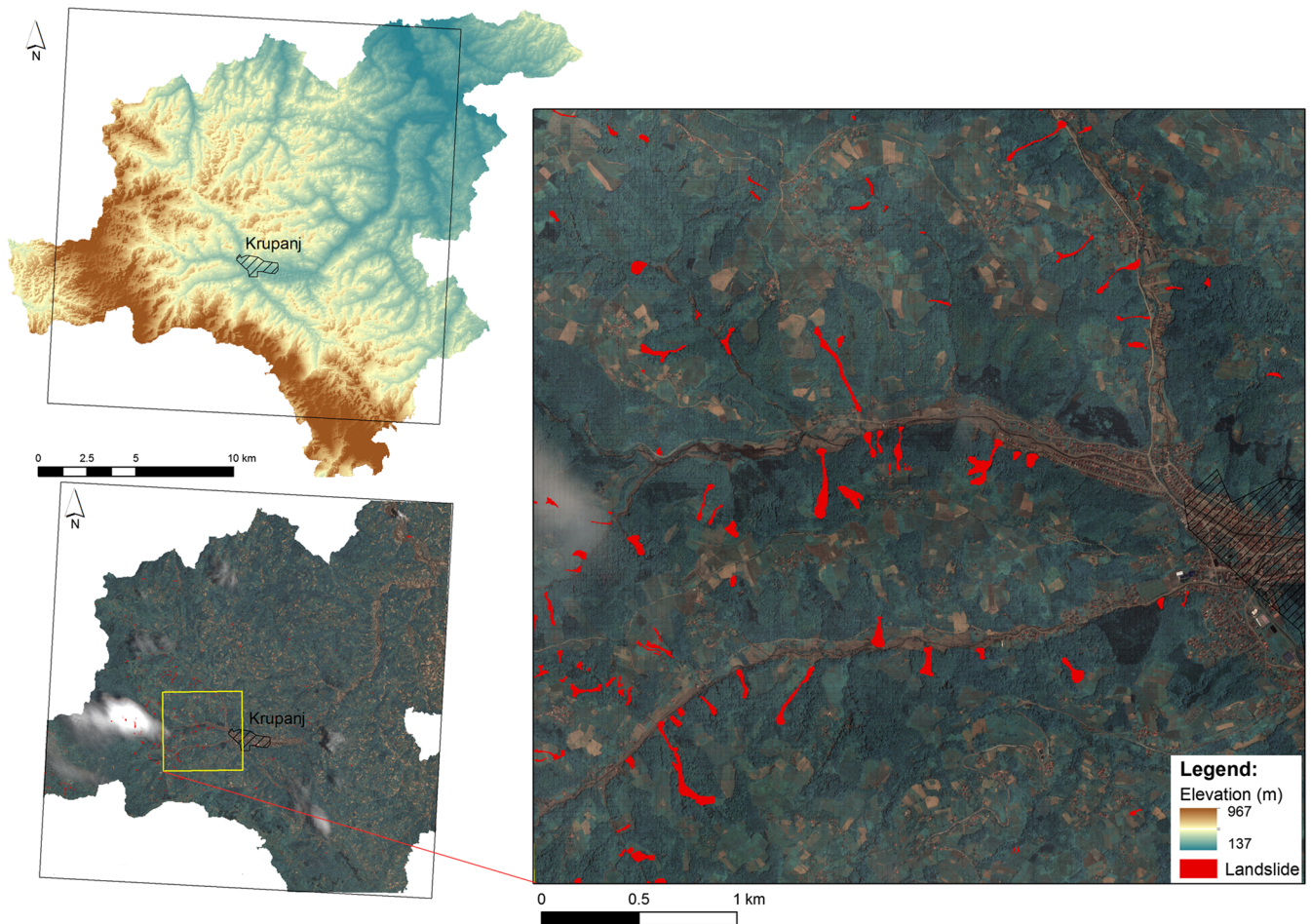Fig. 12 Photo of the he Selanac landslide/debris flow (from Fig. 11)

Fig. 13 An example of visual recognition of landslides (*red colour*) in Krupanj area. Pléiades image, June 8, 2014 (transparency 50%)

field campaign data were concentrated at predefined locations. These locations were chosen based on complaints obtained by the local administration, wherein damage of objects or infrastructure was cited. Processing and inventorying these complaints were necessary for the subsequent financial restitution from the government. The semi-automatic analysis provided results (490 cases of instability) very similar to those of the visual image analysis but lacked the ability to discern between slides and flows.

Conclusion

This research considered the aftermath of a massive landslide event that occurred in May 2014 in Serbia. This study included the 23 municipalities heavily affected by the landslides, as well

as other rainfall-induced calamities. The research objectives focused on two aspects. Firstly, a practical aspect was to provide a reliable landslide inventory that will become a useful support for subsequent field investigations, as well as to observe landslides in inaccessible terrains. Second, a semi-automated analysis was applied over coarser (non-HR/VHR) resolution images that are globally available (Landsat 8 images) to see whether this approach provides any useful information. The idea behind this approach was also a practical one since it entails the use of widely available images to aid field campaigns or directly generates preliminary landslide inventories in a relatively short timeframe, at practically no expense. Given that VHR/HR images are costly and do not have continuous archives (requiring on-demand collection), generating a semi-automated landslide

Table 5 Number of recognized landslides in Krupanj municipality

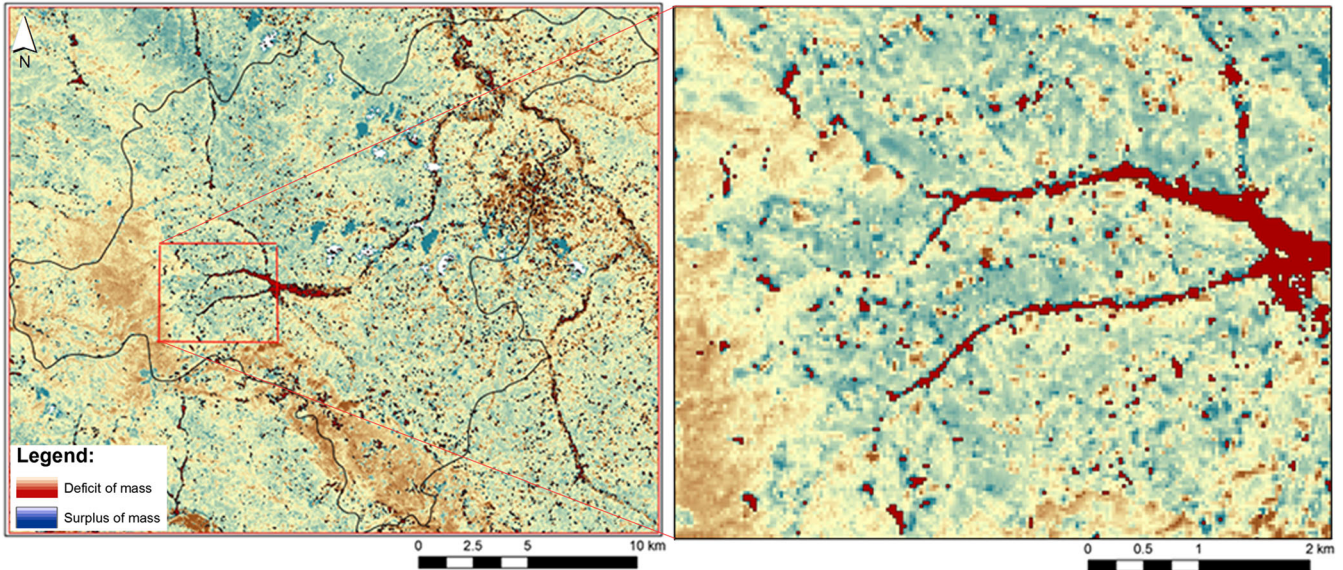| Test area	Number of landslides Visual analysis (Pléiades)	Field observation	Supervised classification (Landsat 8)
Krupanj municipality	507	160	490

Fig. 14 Difference of PCA on pre-event and post-event Landsat 8 images for Krupanj municipality (*red/orange colour* represents deficit of mass, *blue colour* represents surplus of mass)

inventory from coarse resolution but globally available images could attract much attention for critical situations or recovery actions, such as this one.

The results highlighted that the remote sensing-aided approach identified a much higher density of landslides. For instance, the field-based landslide inventory of Krupanj has three times fewer identified landslide occurrences than the visually compiled inventory from the VHR satellite images or the semi-automatically compiled inventory. There is a similar ratio in all other heavily affected municipalities (especially those affected by flows in

central and western Serbia) that had sufficient VHR Pléiades satellite image coverage. It is further shown that semi-automated and visual analyses can have a relatively good overlap (approximately 40%) even with different sources, which means that the landslide recognition criteria were well tuned in both analyses. The poorer results of the field data are, however, a phenomenological and practical matter. Namely, the field work was first conducted to recheck the preliminary inventories provided by the visual and semi-automated analyses, but, following this, the focus of the field campaign was switched to detect slides (confidently recognized
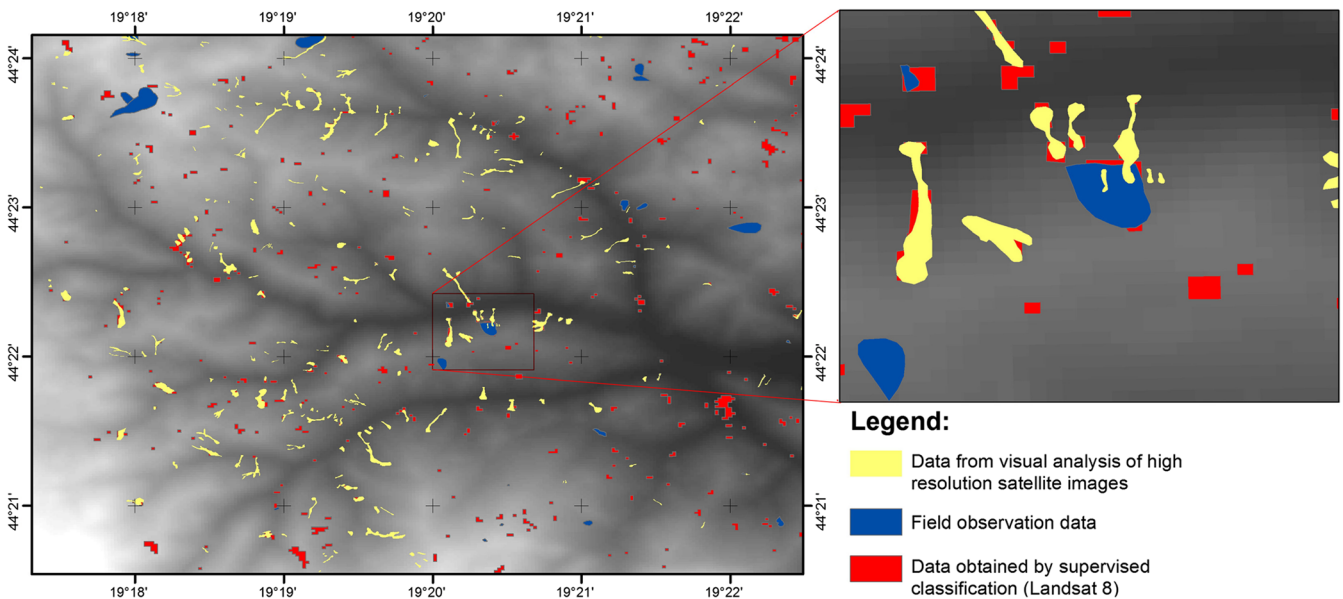

Fig. 15 Interpretation of instabilities based on three types of data (visual analysis of VHR satellite images, *yellow*; field observation data, *blue*; semi-automatic classification of Landsat 8 data, *red*)

only in situ) that had been reported as damaging or threatening by the local authorities of each municipality.

A successful field campaign that resulted in 1785 mapped landslides within 5 months of limited operational activity proves the efficiency of the presented approach and its role in planning detailed research. Reliable inventories, both preliminary and final, are essential for the quality of all subsequent analyses. It is particularly important for event-based inventories because they provide temporal support that can be put to use in a landslide hazard context and in spatiotemporal landslide frequency analysis if enough event-based time splits are collected in the future.

References

Abolmasov B, Milenković S, Marjanović M, Đurić U, Jelisavac B (2015) A geotechnical model of the Umka landslide with reference to landslides in weathered Neogene marls in Serbia. Landslides 12(4):689–702. doi:10.1007/s10346-014-0499-4

Alkevli T, Ercanoglu M (2011) Assessment of ASTER satellite images in landslide inventory mapping: Yenice-Gökçebey (Western Black Sea Region, Turkey). Bull Eng Geol Environ 70:607–617. doi:10.1007/s10064-A011-0353-z.A

Bhambri R, Mehta M, Dobhal DP, Gupta AK, Pratap B, Kesarwani K, Verma A (2016) Devastation in the Kedarnath (Mandakini) Valley, Garhwal Himalaya, during 16–17 June 2013: a remote sensing and ground-based assessment. Nat Hazards 80:1801–1822. doi:10.1007/s11069-015-2033-y

Booth AM, Roering JJ, Perron JJ (2009) Automated landslide mapping using spectral analysis and high-resolution topographic data: Puget Sound lowlands, Washington, and Portland Hills, Oregon. Geomorphology 109:132–147. doi:10.1016/j.geomorph.2009.02.027

Bucknam RC, Coe JA, Chavarria MM, Godt JW, Tarr AC, Bradley L, Rafferty S, Hancock D, Dart L, Johnson ML (2001) Landslides triggered by hurricane Mitch in Guatemala—inventory and discussion. U.S. Geological Survey Open File Report 01-443:39. 23 plates at 1:50,000 scale. http://greenwood.cr.usgs.gov/pub/open-file-reports/ofr-01-0443/

Cardinali M, Galli M, Guzzetti F, Ardizzone F, Reichenbach P, Bartoccini P (2006) Rainfall induced landslides in December 2004 in south-western Umbria, central Italy: types, extent, damage and risk assessment. Nat Hazards Earth Syst Sci 6:237–260

Chavez PS Jr (1996) Image-based atmospheric corrections: revisited and improved. Photogramm Eng Remote Sens 62(9):1025–1036

Chen RF, Chang KJ, Angelier J, Chan YC, Deffontaines B, Lee CT, Lin ML (2006) Topographical changes revealed by high-resolution airborne LiDAR data: the 1999 Tsaoling landslide induced by the Chi–Chi earthquake. Eng Geol 88:160–172. doi:10.1016/j.enggeo.2006.09.008

Ciampalini A, Raspini F, Bianchini S, Frodella W, Bardi F, Lagomarsino D, Traglia F, Moretti S, Proietti C, Pagliara P, Onori R, Corazza A, Duro A, Basile G, Casagli N (2015) Remote sensing as tool for development of landslide databases: the case of the Messina Province (Italy) geodatabase. Geomorphology 249:103–118 http://dx.doi.org/10.1016/j.geomorph.2015.01.029

Cruden DM, VanDine DF (2013) Classification, description, causes and indirect effects—Canadian Technical Guidelines and Best Practices related to Landslides: a national initiative for loss reduction, Geological Survey of Canada Open File 7359

Cruden DM, Varnes DJ (1996) Landslide types and processes. In: Turner AK, Schuster RL (eds) Landslide investigation and mitigation. Special Report 247, Transportation Research Board, National Research Council, National Academy Press, Washington, D.C. 1996, Chapter 3: 36–75

Denis G, de Boissezon H, Hosford S, Pasco X, Montfort B, Ranera F (2016) The evolution of earth observation satellites in Europe and its impact on the performance of emergency response services. Acta Astronautica 127:619–633. doi:10.1016/j.actaastro.2016.06.012

Dimitrijević MD (1997) Geology of Yugoslavia. Gemini-Special Publications, 1–187. Belgrade, ISBN 86-7156–016-3, pp. 1–187

Guzzetti F, Cardinali M, Reichenbach P, Cipolla F, Sebastiani C, Galli M, Salvati P (2004) Landslides triggered by the 23 November 2000 rainfall event in the Imperia Province, Western Liguria, Italy. Eng Geol 73(2):229–245. doi:10.1016/j.enggeo.2004.01.006

Guzzetti F, Mondini AC, Cardinali M, Fiorucci F, Santangelo M, Chang KT (2012) Landslide inventory maps: new tools for an old problem. Earth Sci rev 112:42–66. doi:10.1016/j.earscirev.2012.02.001

Haugerud R, Harding DJ, Johnson SY, Harless JL, Weaver CS, Sherrod BL (2003) High-resolution lidar topography of the Puget Lowland, Washington—a bonanza for earth science. GSA Today 13(6):4–10. doi:10.1130/1052-5173

Hungr O, Leroueil L, Picarelli L (2014) The Varnes classification of landslide types, an update. Landslides 11:167–194. doi:10.1007/s10346-013-0436-y

Iwahashi J, Kamiya I, Yamagishi H (2012) High-resolution DEMs in the study of rainfall- and earthquake-induced landslides: use of a variable window size method in digital terrain analysis. Geomorphology 153–154: 29–38, doi:10.1016/j.geomorph.2012.02.002

Jiménez-Muñoz J, Sobrino J, Gillespie A, Sabol D, Gustafson W (2006) Improved land surface emissivities over agricultural areas using ASTER NDVI. Remote Sens Environ 103:474–487. doi:10.1016/j.rse.2006.04.012

Joyce KE, Samsonov SV, Levick SR, Engelbrecht J, Belliss S (2014) Mapping and monitoring geological hazards using optical, LiDAR, and synthetic aperture RADAR image data. Nat Hazards 73:137–163. doi:10.1007/s11069-014-1122-7

Krstić N, Lj S, Jovanović G, Bodor E (2003) Lower Miocene lakes of the Balkan Land. Acta Geol Hung 46:291–299

Kwan MP, Ransberger DM (2010) LiDAR assisted emergency response: detection of transport network obstructions caused by major disasters. Comput Environ Urban Syst 34:179–188. doi:10.1016/j.compenvurbsys.2010.02.001

Lin CW, Chang WS, Liu SH, Tsai TT, Lee SP, Tsang YC, Shieh CL, Tseng CM (2011) Landslides triggered by the 7 August 2009 Typhoon Morakot in southern Taiwan. Eng Geol 123:3–12. doi:10.1016/j.enggeo.2011.06.007

Lira C, Lousada M, Falcão AP, Gonçalves AB, Heleno S, Matias M, Pereira MJ, Pina P, Sousa AJ, Oliveira R, Almeida AB (2013) The 20 February 2010 Madeira Island flash-floods: VHR satellite imagery processing in support of landslide inventory and sediment budget assessment. Nat Hazards Earth Syst Sci 13:709–719. doi:10.5194/nhess-13-709-2013

Marjanović M, Abolmasov B (2015) Evidencija i prostorna analiza klizišta zabeleženih u maju 2014. Č asopis Izgradnja 69(5–6):129–134 (in Serbian)

Marjanović M, Vulović N, Đurić U, Božanić B (2016) Coupling field and satellite data for an event-based landslide inventory. Proceedings of the 12th International Symposium on Landslides, Naples, Italy, 12–19 June 2016, pp. 1361–1366

Martha TR, Kumar KV (2013) September, 2012 landslide events in Okhimath, India—an assessment of landslide consequences using very high resolution satellite data. Landslides 10(4):469–479. doi:10.1007/s10346-013-0420-6

Martha TR, Kerle N, Jetten V, van Westen CJ, Kumar VK (2010) Characterizing spectral, spatial and morphometric properties of landslides for semi-automatic detection using object-oriented methods. Geomorphology 116(1–2):24–36. doi:10.1016/j.geomorph.2009.10.004

Martha TR, Kerle N, van Westen CJ, Jetten V, Kumar KV (2012) Object-oriented analysis of multi-temporal panchromatic images for creation of historical landslide inventories. ISPRS J Photogramm Remote Sens 67:105–119. doi:10.1016/j.isprsjprs.2011.11.004

Martha TR, Govindharaj KB, Kumar KV (2015) Damage and geological assessment of the 18 September 2011 Mw 6.9 earthquake in Sikkim, India using very high resolution satellite data. Geosci Front 6:793–805. doi:10.1016/j.gsf.2013.12.011

Martha TR, Roy P, Mazumdar R, Govindharaj KB, Kumar KV (2016) Spatial characteristics of landslides triggered by the 2015 Mw 7.8 (Gorkha) and Mw 7.3 (Dolakha) earthquakes in Nepal. Landslides. doi:10.1007/s10346-016-0763-x On-line

Menković L, Koščal M, Mijatović M (2003) Geomorfološka karta Srbije, 1:500 000. Geozavod-Gemini, Belgrade (in Serbian)

Metternicht G, Hurni L (2005) Radu Gogu remote sensing of landslides: an analysis of the potential contribution to geo-spatial systems for hazard assessment in mountainous environments. Remote Sens Environ 98:284–303. doi:10.1016/j.rse.2005.08.004

Mihalić Arbanas S, Arbanas Ž, Abolmasov B, Mikoš M, Komac M (2013) The ICL Adriatic-Balkan Network: analysis of current state and planned activities. Landslides 10:103–109. doi:10.1007/s10346-012-0364-2

Minu NS, Bindhu JS (2016) Supervised techniques and approaches for satellite image classification. International Journal of Computer Applications 134(16):1–6. doi:10.5120/ijca2016908202

Mladenović A, Trivić B, Cvetković V (2015) How tectonic controlled post-collisional magmatism within the Dinarides: inferences based on study of tectono-magmatic events in the Kopaonik Mts. (Southern Serbia). Tectonophysics 646:36–49. doi:10.1016/j.tecto.2015.02.001

Mondini AC, Guzzetti F, Reichenbach P, Rossi M, Cardinali M, Ardizzone F (2011) Semi-automatic recognition and mapping of rainfall induced shallow landslides using satellite optical images. Remote Sens Environ 115:1743–1757. doi:10.1016/j.rse.2011.03.006

Moran S, Jackson R, Slater P, Teillet P (1992) Evaluation of simplified procedures for retrieval of land surface reflectance factors from satellite sensor output. Remote Sens Environ 41:169–184. doi:10.1016/0034-4257(92)90076-V

Murillo-García FG, Alcántara-Ayala I, Ardizzone F, Cardinali M, Fiourucci F, Guzzetti F (2015) Satellite stereoscopic pair images of very high resolution: a step forward for the development of landslide inventories. Landslides 12:277–291. doi:10.1007/s10346-014-0473-1

Osiñska-Skotak K (2007) Studies of soil temperature on the basis of satellite data. International Agrophysics 21(3):275–284

Prohaska S, Đukić D, Bartoš-Divac V, Todorović N, Božović N (2014) Karakteristike jakih kiša koje su prouzrokovale čestu pojavu poplava na teritoriji Srbije u periodu april-septembar 2014.godine. Vodoprivreda 46:15–26 (in Serbian)

Ray PKC, Chattoraj SL, Bisht MPS, Kannaujiya S, Pandey K, Goswami A (2016) Kedarnath disaster 2013: causes and consequences using remote sensing inputs. Nat Hazards 81:227–243. doi:10.1007/s11069-015-2076-0

Sato HP, Harp EL (2009) Interpretation of earthquake-induced landslides triggered by the 12 May 2008, M7.9 Wenchuan earthquake in the Beichuan area, Sichuan Province, China using satellite imagery and Google Earth. Landslides 6:153–159. doi:10.1007/s10346-009-0147-6

Sato HP, Hasegawa H, Fujiwara S, Tobita M, Koarai M, Une H, Iwahashi J (2007) Interpretation of landslide distribution triggered by the 2005 Northern Pakistan earthquake using SPOT 5 imagery. Landslides 4:113–122. doi:10.1007/s10346-006-0069-5

Schefer S (2010) Tectono-metamorphic and magmatic evolution of the Internal Dinarides (Kopaonik area, southern Serbia) and its significance for the geodynamic evolution of the Balkan Peninsula. PhD thesis, University of Basel, Switzerland, p. 234

Schmid MS, Bernoulli D, Fügenschuh B, Matenco L, Schefer S, Schuster R, Tischler M, Ustaszewski K (2008) The Alps-Carpathians-Dinarides-connection: a correlation of tectonic units. Swiss J Geosci 101(1):139–183. doi:10.1007/s00015-008 1247

Schulz WH (2007) Landslide susceptibility revealed by LIDAR imagery and historical records, Seattle, Washington. Eng Geol 89:67–87. doi:10.1016/j.enggeo.2006.09.019

Shafique M, van der Meijde M, Khan MA (2016) A review of the 2005 Kashmir earthquake-induced landslides; from a remote sensing prospective. J Asian Earth Sci 118:68–80. doi:10.1016/j.jseaes.2016.01.002

Tang C, Ma G, Chang M, Li W, Zhang D, Jia T, Zhou Z (2015) Landslides triggered by the 20 April 2013 Lushan earthquake, Sichuan Province, China. Eng Geol 187:45–55. doi:10.1016/j.enggeo.2014.12.004

Tralli DM, Blom RG, Zlotnicki V, Donnellan A, Evans DL (2005) Satellite remote sensing of earthquake, volcano, flood, landslide and coastal inundation hazards. ISPRS Journal of Photogrammetry & Remote Sensing 59:185–198. doi:10.1016/j.isprsjprs.2005.02.002

UNDAC - UN Disaster Assessment and Coordination (2014) End of mission report. United Nations Office for the Coordination of Humanitarian Affairs—OCHA, p. 78, http://reliefweb.int/report/serbia/undac-mission-serbia-floods-18-31-may-2014-end-mission-report. Access Jul 2016

Ustaszewski K, Kounov A, Schmid S, Schaltegger U, Krenn E, Frank W, Fügenschuh B (2010) Evolution of the Adria–Europe plate boundary in the northern Dinarides: from continent-continent collision to back-arc extension. Tectonics 29:TC6017. doi:10.1029/2010TC002668

Valor E, Caselles V (1996) Mapping land surface emissivity from NDVI: application to European, African, and South American areas. Remote Sens Environ 57:167–184. doi:10.1016/0034-4257(96)00039-9

Voigt S, Kemper T, Riedlinger T, Kiefl R, Scholte K, Mehl H (2007) Satellite image analysis for disaster and crisis-management support. IEEE Trans Geosci Remote Sens 45(6):1520–1528. doi:10.1109/TGRS.2007.895830

Xu C, Xu X, Yu G (2013) Landslides triggered by slipping-fault-generated earthquake on a plateau: an example of the 14 April 2010, Ms 7.1, Yushu, China earthquake. Landslides 10:421–431. doi:10.1007/s10346-012-0340-x

Xu C, Xu X, Bruce J, Shyu H, Zheng W, Min W (2014) Landslides triggered by the 22 July 2013 Minxian–Zhangxian, China, Mw 5.9 earthquake: inventory compiling and spatial distribution analysis. J Asian Earth Sci 92:125–142. doi:10.1016/j.jseaes.2014.06.014

Yang X, Chen L (2010) Using multi-temporal remote sensor imagery to detect earthquake-triggered landslides. Int J Appl Earth Obs Geoinf 12:487–495. doi:10.1016/j.jag.2010.05.006

Websites

http://geoliss.mre.gov.rs/beware/, accessed Jul 2016
http://www.regionalnirazvoj.gov.rs/, accessed Jan 2017

D. Đurić · A. Mladenović · M. Pešić-Georgiadis · M. Marjanović ·
B. Abolmasov (✉)
Faculty of Mining and Geology,
University of Belgrade,
Đušina 7, Belgrade, 11000, Serbia
e-mail: biljana.abolmasov@rgf.bg.ac.rs

D. Đurić
e-mail: dragana.djuric@rgf.bg.ac.rs

A. Mladenović
e-mail: ana.mladenovic@rgf.bg.ac.rs

M. Pešić-Georgiadis
e-mail: milica.pesic@rgf.bg.ac.rs

M. Marjanović
e-mail: milos.marjanovic@rgf.bg.ac.rs